UMa Large-Scale O2I Modeling and Base Station Number Optimization

Yutong Wang(✉), Daosen Zhai, Ruonan Zhang, Yi Jiang, and Qi Guo

Department of Communication Engineering, Northwestern Polytechnical University, Xi'an 710072, Shaanxi, China
wangyutong@mail.nwpu.edu.cn

Abstract. The Large-scale fading model of wireless channels plays an important role in the design and analysis of green communication systems and networks. In this paper, we conduct the propagation measurement in the urban macrocell (UMa) outdoor-to-indoor (O2I) scenario at 39 GHz. Based on the field measurement data, we modify the path loss model specified by the 3GPP TR38.901 standard. Furthermore, using the proposed channel model, we analyze the optimal number of base stations (BSs) in a given area to minimize the total power consumption of all the BSs, including both the statistic power and transmitting power. The proposed channel model and optimization solution can be utilized to design green communication systems especially for the millimeter wave wireless networks.

Keywords: outdoor-to-indoor (O2I) · urban macro (UMa) · Green communication

1 Introduction

The outdoor-to-indoor (O2I) coverage is an important application scenario of the mobile communication systems. With the dense deployment of buildings, the O2I channels have become more and more complicated. As a consequence, the previous channel models cannot well depict the propagation properties of the O2I channels especially for the millimeter wave (mmWave) bands. Motivated by the need to improve the channel models, researchers have conducted extensive measurement to investigate and model the O2I channels in different scenarios and frequency bands. For instances, the authors in [1] analyzed the propagation characteristics of the O2I channels at 0.85 and 1.9 GHz, where the transmitter was deployed on the rooftop of several multistory buildings in a university campus. According to the measurement results, it was found that the received

This work was supported in part by the National Natural Science Foundation of China (61571370, 61601365, and 61801388), in part by the Fundamental Research Funds for the Central Universities (3102017OQD091 and 3102017GX08003), and in part by the China Postdoctoral Science Foundation (BX20180262).

B. Li et al. (Eds.): IoTaaS 2018, LNICST 271, pp. 393–400, 2019.
https://doi.org/10.1007/978-3-030-14657-3_40

power at 1.9 GHz was 10 dB smaller that at 0.85 GHz. The authors in [2] studied the wireless channels at 3, 10, 17, and 60 GHz in an O2I scenario. The results revealed that the signal attenuation fluctuated significantly, depending on the materials of the windows. In [3], the 2.6 GHz O2I channel was characterized for the tunnel and open field environments in subways. The results indicated that the attenuation values were 15 to 20 dB higher than those in free space, due to the non-line-of-sight (NLOS) propagation. The penetration capabilities of the linear polarization (LP) and circular polarization (CP) were compared in [4]. The analysis found that the CP had more parallel polarization components and hence it had a stronger penetration capability with respect to the LP in most O2I scenarios.

The fifth generation (5G) mobile communication networks is undergoing standardization. The 5G is expected to meet the user requirement for ultra-high data rates, but at the expense of increased cost [5]. The network will include a plenty of base stations (BSs), mobile devices, and antennas [6]. Therefore, it is necessary to properly deploy BSs to reduce energy consumption. A fairness-aware multiple drone base stations (DBS) deployment algorithm was proposed in [7], which could maximize the proportional fair sum-rate by using the particle swarm optimization (PSO). The results were provided for the downlink coverage probability of a wireless network with predetermined BS locations in [8]. The authors proposed a chance-constrained stochastic formulation for the optimal network deployment.

This paper focuses on the large-scale O2I channel analysis and modeling at 39 GHz in the mmWave band. Specifically, we have performed a channel measurement campaign in a typical urban macrocell (UMa) scenario, and then modified the model parameters in the 3GPP TR38.901 standard to improve the accuracy based on our measurement data. Furthermore, in order to reduce the energy consumption of the mmWave network, we analyze the optimal number of BSs in a given area based on the modified large-scale channel fading model. Simulation results indicate that the total power consumption of all BSs can be minimized through optimizing the BS density.

The rest of the paper is organized as follows. Section 2 introduces the channel measurement scenario and system. Section 3 presents the measurement results and the proposed path loss model. In Sect. 4, we analyze the optimal number of BSs for the network deployment. Finally, Sect. 5 concludes the paper and points out the future research issues.

2 Channel Measurement Scenario and System

2.1 Measurement Scenario

The channel measurement campaign was carried out at the Minhang campus of Shanghai Jiao Tong University, which was a typical UMa O2I scene. As shown in Fig. 1, the transmitter (Tx) was installed on a five-story building with a height of about 24 m, and the antenna height was about 25 m above the ground. The receiver (Rx) was located on the second and third floors in an adjacent building.

The floorplan of the measured positions is shown in Fig. 1(c). The height of the receiving antenna was 1.5 m high a total of 61 positions on the second floor and 58 positions on the third floor were measured.

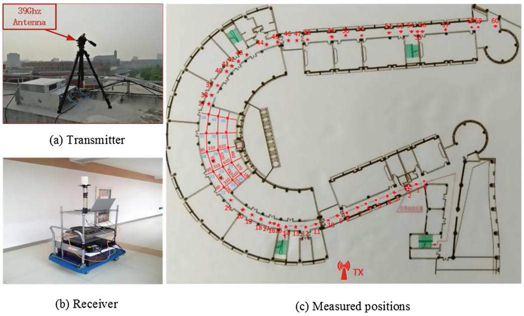

Fig. 1. Transceiver and measurement scenarios.

2.2 Measurement System

The block diagram of the large-scale channel sounding system is shown in Fig. 2. The Tx consists of a signal source, a high-frequency power amplifier (PA), a transmitting antenna, and connection cables. The transmitting antenna is sectorial with a half power beam width (HPBW) of 60°. The Tx is powered by the municipal electricity due to the huge power consumption of the amplifier. The Rx is composed of a UPS power supply device, a handheld GPS device, a spectrum analyzer, a receiving antenna, a laptop computer, and connection cables. An omnidirectional cylindrical antenna is used in the Rx.

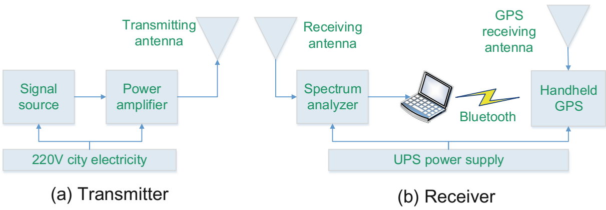

Fig. 2. Block diagram of the large-scale channel measurement system.

The transmitting power of the signal source is 10 dBm, and the gain of the high-frequency power amplifier is 63 dB. The gain of the Tx and Rx antennas are 8.5 and 2.5 dBi, respectively. The spectrum analyzer is connected to the laptop through a Category 5 network cable. The handheld GPS device records the positions of the Rx, and sends the information to the laptop through Bluetooth to calculate the three-dimensional Tx-Rx distance in the data processing.

2.3 Measurement System Calibration

In order to obtain accurate path loss in the measurement, the entire measurement system must be calibrated, including connection cables, antennas, power amplifiers, and so on. The patterns of the Tx and Rx antennas have been measured in a microwave anechoic chamber. Specifically, the system is calibrated by the back-to-back calibration method. The Tx and Rx are connected directly with cables. Since the output power of the power amplifier is very large, an attenuator with a predetermined attenuation coefficient is inserted between the power amplifier and the spectrum analyzer. To minimize the measurement error, the same transmission power and high-frequency phase-steady cables in the calibration process are used in the field measurement. The block diagram of the calibration process is shown in Fig. 3. The symbol definition is summarized in Table 1.

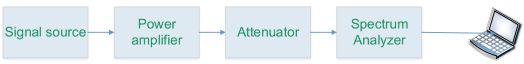

Fig. 3. Calibration operating system block diagram.

Table 1. The symbol definitions.

Symbols	Meanings
P_{TX} (dBm)	The transmitting power of the signal source
G_{PA} (dBm)	The gain of the power amplifier
G_A (dB) > 0	The attenuation coefficient of the attenuator
G_{TX}	The gain of the Tx antenna
G_{RX}	The gain of the Rx antenna
P_{RX1}	The received signal power of the spectrum analyzer in calibration
P_{RX2}	The received signal power of the spectrum analyzer in field measurement
PL	The path loss of the wireless channel
L	The other loss of the measurement system

According to the calibration diagram, we can obtain.

$$P_{TX} + G_{PA} - G_A - L = P_{RX1}. \tag{1}$$

$$P_{TX} + G_{PA} + G_{TX} - PL + G_{RX} - L = P_{RX2}. \tag{2}$$

Substituting (1) into (2) yields

$$PL = P_{RX1} - P_{RX2} + G_A + G_{TX} + G_{RX}. \tag{3}$$

In order to verify the channel sounding system and the calibration scheme, we conducted a field measurement experiment. The experiment was performed in an open space to emulate the free-space scenario. The, Tx-Rx distance was set as 5, 10, and 15 meters for air interface testing. The path loss was obtained by using (3). The experimental results indicate that the errors between the measurement results and the free-space model were between 0.6–1.1 dB, within the allowable range.

3 Measurement Results and Modeling

Path loss is one of the large-scale fading parameters of wireless channels. This paper models the path loss at 39 GHz in the UMa scenario based on the field measurement data and the 3GPP TR 38.901 standard. The path loss model is expressed as

$$PL = PL_b + PL_{tw} + PL_{in} + N(0, {\sigma_p}^2), \tag{4}$$

$$PL_b = 28 + 23.46 \cdot \log_{10}(d_{3D}) + 21.23 \cdot \log_{10}(f_c), \tag{5}$$

$$PL_{in} = 0.5 d_{2D\_in}, \tag{6}$$

where PL_b is the basic outdoor path loss given in (5), PL_{in} is the indoor loss depending on the depth into the building and given in (6), and d_{2D_in} is 2D distance between Tx and Rx. In (4), σ_p=4.4 is the standard deviation of the penetration loss. PL_{tw} is the building penetration loss through the external wall given by

$$\begin{aligned} PL_{tw} &= PL_{npi} - 10\log_{10} \sum_{i=1}^{N} P_i \times 10^{\frac{-L_{material\_i}}{10}} \\ &= 5 - 10\log_{10}(0.9 \cdot 10^{\frac{-L_{concrete}}{10}} + 0.05 \cdot 10^{\frac{-L_{glass}}{10}} + 0.05 \cdot 10^{\frac{-L_{wood}}{10}}), \end{aligned} \tag{7}$$

$$L_{glass} = 2 + 0.2 f_c, \tag{8}$$

$$L_{concrete} = 5 + 4 f_c, \tag{9}$$

$$L_{wood} = 4.85 + 0.12 f_c, \tag{10}$$

where PL_{npi} is an additional loss added to the external wall loss to account for non-perpendicular incidence, P_i represents the proportion of the i-th material, where $\sum_{i=1}^{N} P_i = 1$, and N is the number of materials.

The measurement data and our model are depicted in Fig. 4, where (a) represents the path loss in the second floor and (b) represents the path loss in the third floor. As can be seen, our model can well match the measurement data. The positions of 9, 10, 46, and 47 shown in Fig. 1 have line-of-sight (LOS) rays, and thus their path loss is relative small. For these positions, we do not add the penetration loss into the path loss model.

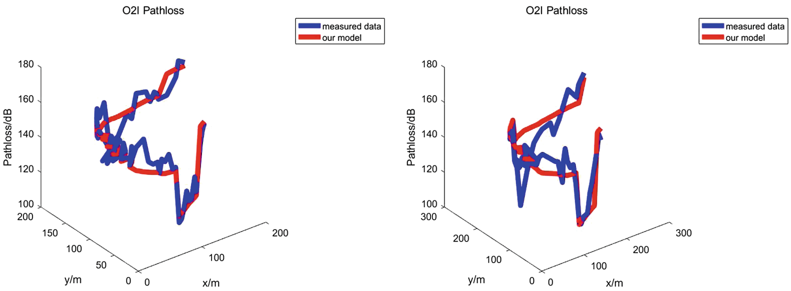

(a) Second floor (b) Third floor

Fig. 4. Measured data and our model

4 Base Station Deployment OPTIMIZATION

The power consumption of a base station (BS) consists of two parts, i.e., the transmitting power and the statistic power. Given a network coverage area, with the increment of the number of BSs, the radius of the coverage area of a BS decreases. As a result, the transmitting power may be reduced to satisfy the minimum received power requirement P_r. On the contrary, the smaller the number of BSs is the larger the transmitting power is consumed, but the smaller statistic power is required. As such, there is a tradeoff between the transmitting and statistic power by changing the number of BSs. In other words, there is an optimal three-dimensional distance between the cell-edge user and the BSs, which can minimize the total power consumption of all BSs. Suppose that the geographic area is defined as S. The height of the BS is h. We denote P^c and P^t as the statistic and transmitting power, respectively. Specifically, the BS coverage is shown in Fig. 5.

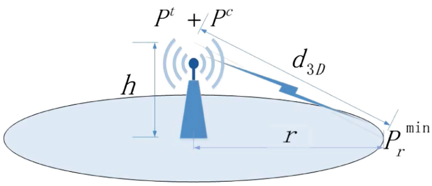

Fig. 5. Base station coverage.

The mathematical analysis for the optimal d_{3D} is given as follows. The BS height h and coverage radius r are known, and thus the three-dimensional distance from the user to the BS d_{3D} is obtained as

$$d_{3D}{}^2 = h^2 + r^2. \tag{11}$$

The total area is divided by the coverage area of the BSs and the number of BSs, denoted by N_b, is obtained as

$$N_b(d_{3D}) \approx \frac{S}{\pi r^2} = \frac{S}{\pi({d_{3D}}^2 - h^2)}. \tag{12}$$

The summation of the minimum received power and the path loss gives the dynamic transmitting power of the i-th BS, denoted by P_i^t, as

$${P_i}^t(d_{3D}) = {P_r}^{\min} + PL(d_{3D}). \tag{13}$$

The total power is the summation of the static and transmitting power of all the N_b BSs and can be obtained as

$$\begin{aligned} P^{tot}(d_{3D}) &= \sum_{i=1}^{N_b(d_{3D})} ({P_i}^c + {P_i}^t(d_{3D})) \\ &= \sum_{i=1}^{\frac{S}{\pi({d_{3D}}^2 - h^2)}} ({P_i}^c + {P_r}^{\min} + PL(d_{3D})), \end{aligned} \tag{14}$$

where P^{tot} is the total power, and P_i^c is the BS static power.

The total power minimization problem can be formulated as

$$\begin{aligned} &\min_{d_{3D}} P^{tot}(d_{3D}) \\ &s.t. \quad d_{3D} > h \end{aligned} \tag{15}$$

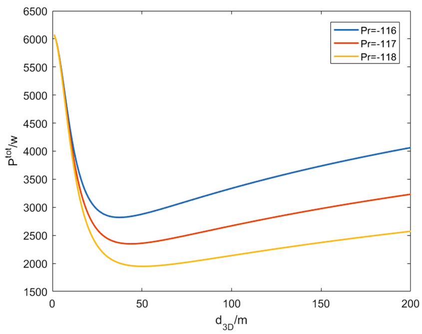

Fig. 6. The effect of the 3D-distance on the total power consumption.

In this work, we solve the problem via numerical results. Specifically, we set h = 12.5 m, P^c = 30 watt, and $S = 10^5$ m^2. The relationship between the total power of the BSs and the three-dimensional distance from the edge users to a BS is shown in Fig. 6. The vertical distance between the Tx and the Rx is set by the path loss model. From Fig. 6, we can find that with under different minimum received power (MRP) requirements, the optimal d_{3D} and the optimal number of BSs vary. For example, when MRP is −116 dBm, the optimal d_{3D} is 37 m, and the corresponding number of BSs is 26. When MRP is −118 dBm, the optimal d_{3D} is 53 m, and the corresponding number of BSs is 12.

5 Conclusions

In this paper, we have measured the 39 GHz large-scale fading in the typical UMa O2I scenario. Based on the measurement data, we have modified the parameters in the 3GPP TR38.901 standard to improve the channel model for the O2I mmWave channels. Moreover, by using the proposed channel model, we have evaluated the optimal number of BSs for a given coverage area to minimize the total power consumption. Our study provides guidance for the green networking of the 5G system, especially for the mmWave O2I coverage. In the future works, we will perform more field measurement on the mmWave channels such as in the urban microcell (UMi) and indoor scenarios, to provide more measurement data to refine the channel models for network deployment.

References

1. Calderon Jimenez, M.J., Arana, K., Arias, M.R.: Outdoor-to-indoor propagation mechanisms in multistorey building for 0.85 GHz and 1.9 GHz bands. In: IEEE 37th Central America and Panama Convention (CONCAPAN XXXVII), Managua, pp. 1–6 (2017)
2. Diakhate, C.A.L., Conrat, J.M., Cousin, J.C., Sibille, A.: Millimeter-wave outdoor-to-indoor channel measurements at 3, 10, 17 and 60 GHz. In: 2017 11th European Conference on Antennas and Propagation (EUCAP), Paris, pp. 1798–1802 (2017)
3. Arriola, A., Briso, C., Moreno, J., Echeverria, E.: Characterization of an outdoor-to-indoor wireless link in metro environments at 2.6 GHz. In: 2017 15th International Conference on ITS Telecommunications (ITST), Warsaw, pp. 1–4 (2017)
4. Zhong, Z., Liao, X.: Circular polarization benefits in outdoor to indoor scenarios for MIMO cellular networks. In: 2014 6th International Conference on Wireless Communications and Signal Processing (WCSP), Hefei, pp. 1–5 (2014)
5. Gandotra, P., Jha, R.K., Jain, S.: Green communication in next generation cellular networks: a survey. IEEE Access **5**, 11727–11758 (2017). https://doi.org/10.1109/ACCESS.2017.2711784
6. Andrews, J.G., et al.: What will 5G Be? IEEE J. Sel. Areas Commun. **32**(6), 1065–1082 (2014)
7. Akarsu, A., Girici, T.: Fairness aware multiple drone base station deployment. IET Commun. **12**(4), 425–431 (2018)
8. Chatterjee, S., Abdel-Rahman, M.J., MacKenzie, A.B.: Optimal base station deployment with downlink rate coverage probability constraint. IEEE Wirel. Commun. Lett. **7**(3), 340–343 (2018)